

Article

Design and Implementation of a New Algorithm for Enhancing MPPT Performance in Solar Cells

Ehsan Norouzzadeh ¹, Ahmad Ale Ahmad ², Meysam Saeedian ³ , Gholamreza Eini ⁴ and Edris Pouresmaeil ^{3,*} 

¹ Department of Electrical and Computer Engineering, Semnan University, Semnan 35131-19111, Iran; e.norouzzadeh@semnan.ac.ir

² Department of Electrical and Computer Engineering, Babol Noshirvani University of Technology, Babol 47148-71167, Iran; a.ahmad@nit.ac.ir

³ Department of Electrical Engineering and Automation, Aalto University, 02150 Espoo, Finland; meysam.saeedian@aalto.fi

⁴ Department of Electrical and Computer Engineering, Arak University of Technology, Arak 38181-41167, Iran; gholamrezaeini1371@gmail.com

* Correspondence: edris.pouresmaeil@aalto.fi

Received: 3 December 2018; Accepted: 30 January 2019; Published: 6 February 2019



Abstract: This paper presents a new algorithm for improving the maximum power point tracking method in solar cells. The perturb and observe and the constant voltage algorithms are combined intelligently in order to have a fast response and a high power efficiency. Furthermore, a two-phase interleaved boost converter with a coupled inductor is used with the proposed algorithm. The input capacitor and inductor of this converter are much smaller than those of the conventional types of converters. Therefore, its inherent delay is too short. Computer simulations carried out in PowerSIM and experimental results using a 100 W prototype verify the superior performance of the proposed algorithm and converter. The operating principle and comparisons with the conventional algorithms and other methods are presented in this paper. Moreover, a cost function is presented to compare the new algorithm with the others. The experimental results show that the presented system tracks any changes in power in less than 10 ms, and a quick response to the maximum power point is achieved.

Keywords: solar cells; maximum power point tracking; solar energy conversion

1. Introduction

Fossil fuels are the major energy source that is declining over time and is also creating many problems such as air pollution. Therefore, a great energy transition from fossil fuels to renewable energy sources, particularly solar energy, is underway [1,2]. Nonetheless, the efficiency of solar cells (SCs) is low, and power delivery depends on ambient irradiation and temperature. Therefore, it is necessary to extract the maximum available power from SC. There are several techniques to track the maximum power point, which are known as maximum power point tracking algorithms.

The perturb and observe (P&O) is the most popular maximum power point tracking (MPPT) algorithm [3,4]. In this algorithm, the output power is calculated in each cycle by sampling the current and voltage of the SC. Then, according to the difference between the current output power and the output power of the previous cycle, the operating point of the SC is modified to achieve the maximum power point (MPP). Cheapness and low complexity are two advantages of using P&O. It also does not depend on the characteristics of the SC. However, its response is slow and oscillates around the MPP, especially when temperature or irradiation change extremely. An adaptive P&O algorithm is suggested in Reference [5]. This algorithm consists of two parts: (1) the current perturbation algorithm

and (2) the adaptive control algorithm. These two parts are based on the conventional P&O and fractional short-circuit current algorithms. In References [6,7], a modified P&O algorithm is used to improve the MPPT.

Another algorithm is the incremental conductance (IC) algorithm [4,8]. The IC algorithm is based on the fact that the power slope of the SC at the MPP is zero ($dP/dV = 0$). In this algorithm, incremental conductance (dI/dV) is compared with the instantaneous conductance (I/V) in each cycle, and the operation point of the SC is moved to the MPP. The IC algorithm is similar to the P&O, except that it presents better responses; however, its calculation is more complex. In Reference [9], a novel variable step-size incremental-resistance MPPT algorithm is introduced, which atomically adjusts the step size to track the MPP. This algorithm improves the steady-state and dynamic response and has a wide operating range.

Constant voltage (CV) is an algorithm that is very simple to implement [10,11]. In the CV algorithm, a fixed reference voltage (V_{ref}) regulates the output voltage of the SC. The V_{ref} is constant and is extracted from the characteristics of the SC. Therefore, the operating point of the SC is always kept near the MPP. A simple implementation and a fast response are the advantages of CV, but it cannot find the exact MPP. In Reference [12], an adaptive voltage sensor is presented. This method uses a variable scaling factor and a direct duty cycle control method, can determine the voltage by a voltage divider circuit and can improve the transient and steady-state performance, without employing a PI controller.

Fraction open-circuit voltage (V_{OC}) is another MPPT algorithm [8]. In this algorithm, V_{MPP} is calculated as:

$$V_{MPP} = k \times V_{OC} \quad (1)$$

where k is usually between 0.7 and 0.9. This algorithm is simple, but its accuracy is low, and determining best value of k is difficult. In Reference [13], a fuzzy agent adapted with the fractional open-circuit voltage technique is used to track the MPP in a fast and accurate manner.

The reaction short-circuit current (I_{SC}) algorithm is similar to the open-circuit algorithm [14]. In this algorithm, the SC current is used to calculate the current at maximum power (I_{MPP}) as follow:

$$I_{MPP} = k \times I_{SC} \quad (2)$$

This algorithm is more expensive than the fractional open-circuit voltage algorithm. In Reference [13], a modified fractional short-circuit current MPPT algorithm is introduced on the basis of the determination of the optimum slope of the power load line.

Moreover, some methods are based on a mathematical function. In Reference [14], a complex function is introduced in order to track the maximum power point. The function is formed by a two-dimensional Gaussian function and an arctangent function with an adaptive perturbation step size. In Reference [15], a parameter-estimation-based MPPT method for the power of photovoltaic generation, based on the measured voltages, currents, and the characteristics of the output function of photovoltaic generation (PVG) is presented. The proposed MPPT method uses parameter estimations to directly calculate the solar irradiance and temperature.

The neural network and the fuzzy logic controllers, which provide faster tracking of MPP and present smoother signals with less fluctuation, are expensive and have high implementation complexity [16,17]. In Reference [18], a new digital control scheme using a fuzzy-logic and a dual MPPT controller is introduced. This paper employs the P&O algorithm, and in order to eliminate the resulting state oscillations, the fuzzy logic controller is gradually updated. In Reference [19], to decrease the energy loss in the MPPT circuit, a successive approximation register method that has a power-down mode is proposed, based on a hill climbing algorithm with a fast-tracking time. This MPPT technique specifies the direction of the perturbation and employs the binary search method of the successive approximation.

Besides the methods mentioned above, many other methods are employed. In Reference [20], a new method of tracking the MPP of a photovoltaic module is presented, which exploits the effects of the inherent characteristic resistances of the PV cells. An analysis of the IV characteristics of the photovoltaic module in the IV plane revealed the possibility of predicting the MPP by finding the maximum possible power rectangle within an analysis of the IV characteristics. In Reference [21], a robust input–output linearization controller that establishes a linear mapping between the duty cycle and the SC voltage is proposed. This method consists of a dynamic assignment and linearizing control. In Reference [22], to improve time tracking and MPPT efficiency, an adaptively binary-weighted step and a monotonically decreased step are used.

This paper proposes a new MPPT algorithm in order to obtain a fast and accurate response in solar cells. The new algorithm is an intelligent combination of the P&O and the CV algorithms (CPV). When the irradiation changes suddenly, the operation point gets close to the MPP using the CV algorithm. Then, the P&O algorithm will find the new MPP, exactly. A two-phase interleaved boost converter with a coupled inductor is used because of its much greater reduction of the input switching current ripple. Therefore, an interleaved boost converter (IBC) does not need a bulk input capacitor. The successful performance of the MPPT algorithm is verified through a simulation and the related experimental results.

2. Solar Cell

SCs are electrical devices that convert the sun's energy directly into electricity, when exposed to sunlight. A SC is a positive-negative (PN) junction with a large surface area which allows light to pass through the PN junction. Thus, its mathematical equation is represented by [23]:

$$I_D = I_{rs} \left(e^{qV/kT} - 1 \right) - I_L \quad (3)$$

where I_D is the diode current (A), I_L is the light generated current (A), I_{rs} is the diode saturation current (A), q is the electron charge (1.6×10^{-19} C), k is the Boltzmann constant (1.38×10^{-23} J/K), and T is the cell temperature (K). This equation can be considered as having two parts: the current described by the usual diode equation and the current due to the light generation. The power delivered from the diode and solar energy is then converted into electricity when the diode begins to shift down into the fourth quadrant. The physical model of a solar cell including the current source, diode, and parallel and series resistance is shown in Figure 1.

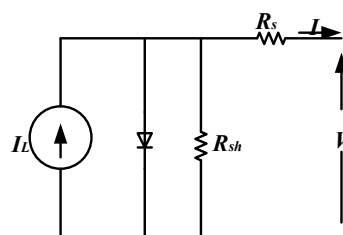


Figure 1. Physical model of the solar cell (SC).

The basic equation describing the model of a solar cell is as follows [3,16]:

$$I = I_L - I_{rs} \left(e^{\frac{q(V+IR_s)}{KT}} - 1 \right) - \frac{V + IR_s}{R_{sh}} \quad (4)$$

where (V) and (I) are the cell voltage (V) and the current (A), respectively. (R_s) is the equivalent series resistance, and (R_{sh}) shows the parallel resistance. The ' I - V ' characteristic of a typical SC is shown in Figure 2a.

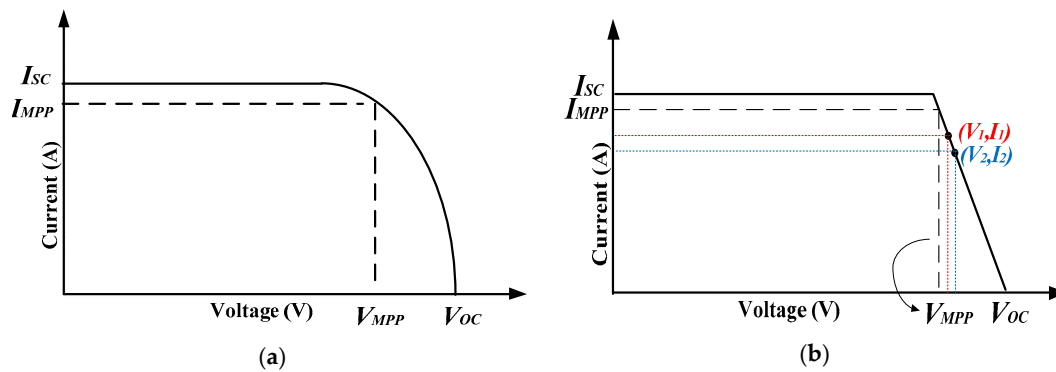


Figure 2. SC current versus voltage characteristic; (a) is the actual curve, (b) is the approximate curve.

3. Proposed MPPT Algorithm

3.1. CPV Algorithm

The P&O and the CV algorithms are two popular MPPT algorithms because of their simplicity, cheapness, and independence from the environmental conditions. The response of the P&O algorithm is very slow, but the exact MPP can be found, and the output power ripple is very small around the MPP. On the other hand, the CV response is fast, but it can only keep the operation point near the MPP. Figure 3a,b show the P&O and CV algorithm performances for different irradiation levels, respectively. Let us assume that the SC is at point A (MPP of curve 1) and that suddenly the irradiation reduces to curve 2. If the P&O algorithm is used, the operation point reaches the point C, far from the MPP of curve 2. Then, the P&O algorithm will move slowly to the operation point to B (MPP of curve 2). In addition, the return trajectory is B→D→A when the irradiation increases to curve 1. In the CV algorithm, when the irradiation reduces to curve 2, the operation point reaches point E. E is not the MPP at the new irradiation but it is close to point B (MPP of curve 2), as shown in Figure 3b.

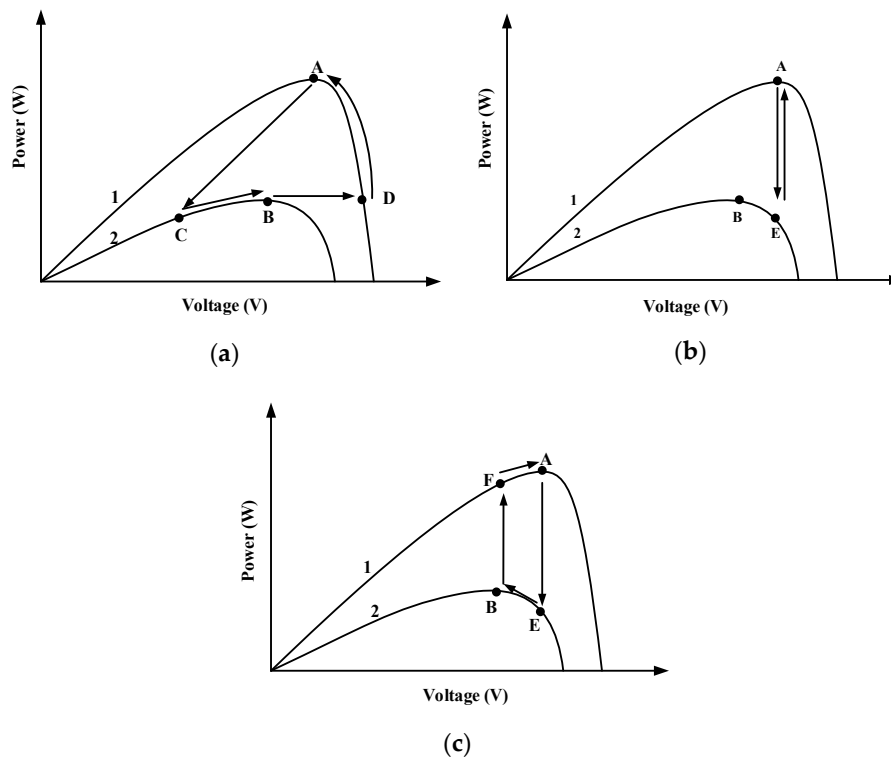


Figure 3. Maximum power point tracking by using (a) the perturb and observe (P&O) algorithm, (b) the constant voltage (CV) algorithm, (c) the proposed algorithm.

The proposed algorithm uses both the P&O and the CV algorithms. Figure 3c shows the trajectory of the SC operation point under the proposed algorithm. In this algorithm, when the irradiation changes suddenly, the operation point gets rapidly closer to the MPP by the CV algorithm. Then, P&O will find exactly where the new MPP is. Figure 4 shows the flowchart of the proposed algorithm. According to Figure 4, if the irradiation changes strongly and ΔP is larger than ΔP_{max} , then V_{ref} will stay fixed, otherwise the P&O will not perform reliably. In the proposed algorithm, the selection of ΔP_{max} is an important issue. It depends on the characteristics of the SC and the weather conditions. However, a good selection will be as follows:

$$\Delta P_{max} = 0.04 \times \text{maximum power of SC} \tag{5}$$

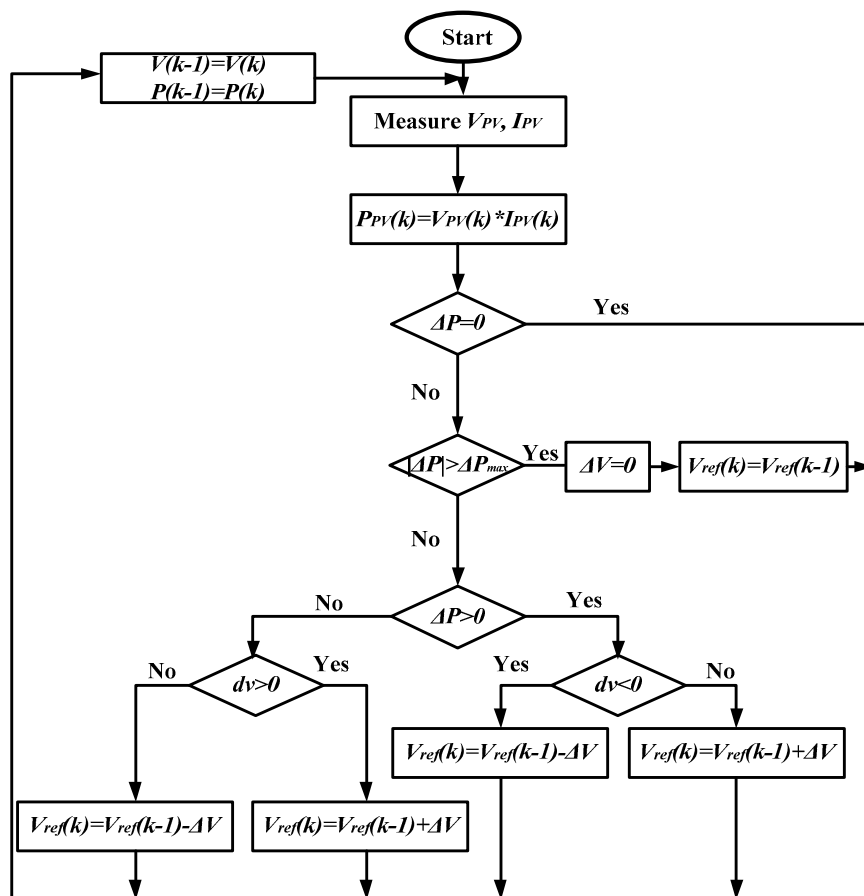


Figure 4. Flowchart of the proposed algorithm.

3.2. Selection of ΔV

Correct ΔV selection is very important in order for the P&O algorithm to perform reliably. ΔV is the voltage moving step to the MPP. If it is selected very small, the MPP will be fixed exactly, but the response time of the algorithm will be slow. To decrease the response time, a large ΔV should be selected. A larger ΔV will lead to a higher oscillation of the operation point around the MPP. Therefore, the relation between ΔV and ΔP is important. As shown in Figure 2b, if the solar cell current–voltage relationship is estimated to be represented by straight lines, the operation points 1 and 2 (near MPP) are expressed as:

$$I_1 = m(V_1 - V_{OC}) \tag{6}$$

$$I_2 = m(V_2 - V_{OC}) \tag{7}$$

where

$$m = \frac{-I_{MPP}}{V_{OC} - V_{MPP}} = \frac{-I_{MPP}}{V_{OC}(1 - k)} \tag{8}$$

The power difference between the two points, ΔP , will be

$$\Delta P = V_2 I_2 - V_1 I_1 \tag{9}$$

Substituting Equations (6) and (7) into Equation (8) gives the following:

$$\Delta P = V_2 m (V_2 - V_{OC}) - V_1 m (V_1 - V_{OC}) = m V_2^2 - m V_2 V_{OC} - m V_1^2 + m V_1 V_{OC} = m (V_2^2 - V_1^2) + m V_{OC} (V_1 - V_2) \tag{10}$$

Equation (10) can be rearranged as follows:

$$\Delta P = m (V_2 - V_1) (V_2 + V_1) + m V_{OC} (V_1 - V_2) \tag{11}$$

The voltage difference ΔV is defined as

$$\Delta V = V_2 - V_1 \tag{12}$$

Thus, substituting Equation (10) into Equation (9) gives

$$\Delta P = \Delta V (m (V_2 + V_1 - V_{OC})) \tag{13}$$

Since V_1 and V_2 are smaller than V_{OC} :

$$\Delta P \leq \Delta V \times m \times V_{OC} \tag{14}$$

Therefore, Equation (14) can be written in the following form:

$$\Delta V \geq \frac{\Delta P}{m \times V_{OC}} \tag{15}$$

Therefore, the relation between ΔP and ΔV can be obtained from Equation (15).

3.3. Boost Converter

As shown in Figure 5, a boost converter is usually used for solar systems because of the continuous input current. However, it suffers from the inherent switching ripple. In a conventional boost converter, the input current ripple is between 30 to 60% of the nominal input current, as shown in Figure 6. This ripple causes a large power ripple in solar cells, which is unfavorable for solar systems.

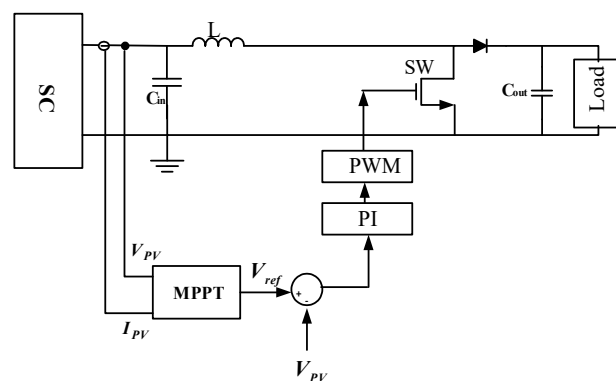


Figure 5. SC system configuration (PWM: pulse width modulation, PI: proportional–integral controller, SW: switch).

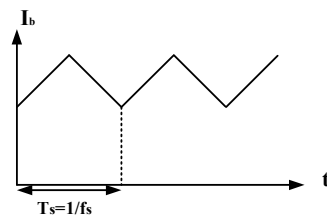


Figure 6. Input current ripple of a non-isolated boost converter in continuous current mode.

As shown in Figure 7, to resolve this problem, a very bulk electrolyte capacitor or inductor is often connected to the input of boost converter. This solution increases the inherent delay of the boost converter, because they are energy-storage elements. While the response time of a boost converter is slow, it cannot be expected from the MPPT algorithm to have a fast response. In addition, there is a limitation on the lifespan of the bulk electrolyte capacitor.

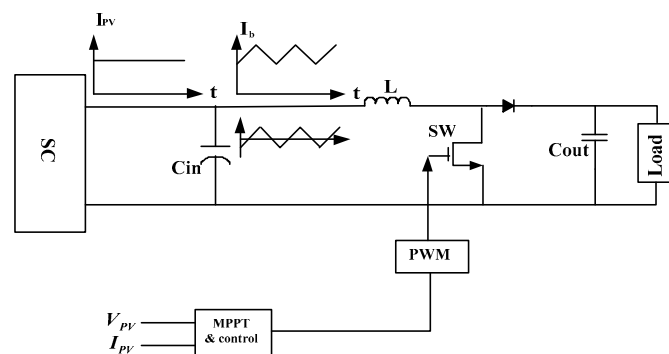


Figure 7. SC with an added input capacitor.

Another solution to reduce the input current ripple is using an interleaved boost converter (IBC). The n-phase interleaved boost converters are driven at $360/n$ degrees out of phases. Thus, the input effective switching current ripple is very largely reduced, because the n-phases are combined together. Therefore, an IBC does not need a bulk input capacitor. An IBC can improve the conversion efficiency and minimize switching losses, too. Thus, the IBC overcomes the drawbacks of the conventional boost converter.

In the proposed method, a two-phase interleaved boost converter with coupled inductor was employed. The coupled inductor distributed the input current equally, and the inherent current was not returned. The IBC is shown in Figure 8.

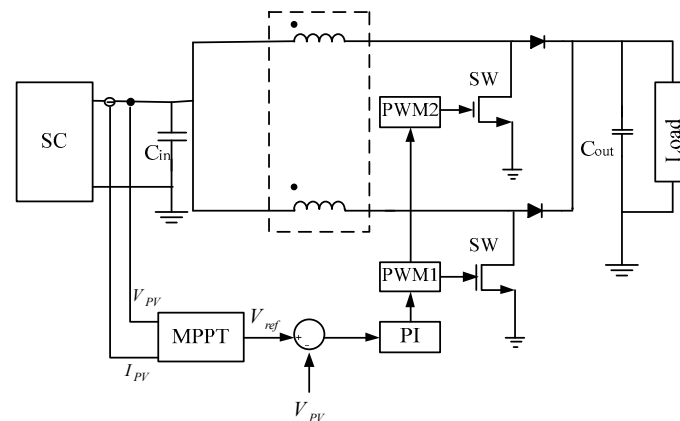


Figure 8. Block diagram of the interleaved boost converter (IBC) used in the proposed method for the SC system.

4. Analysis of the Simulation and Experimental Results

The proposed algorithm and the IBC were verified by a simulation and related experimental results from a 100 W prototype. The solar cell and boost converter parameters are listed in Tables 1 and 2.

Table 1. Characteristics of the 100 W solar cell.

Symbol	Quantity	Value
PMPP	Maximum power	100 W
VMPP	Voltage at maximum power	20.45 V
IMPP	Current at maximum power	4.89 A
VOC	Open circuit voltage	25 V
ISC	Short circuit current	5.19 A
α ISC (%/0C)	Current temperature coefficient	0.024
β VOC (%/0C)	Voltage temperature coefficient	-0.356

Table 2. Specification of the boost converter.

Symbol	Quantity	Value
V_{in}	Input voltage	15–25 V
V_{out}	Output voltage	26–30 V
I_{max}	Maximum input current	6 A
f_{sw}	Switching frequency	12 KHz
C_{in}	Input capacitor	1 μ F
L	Inductance	370 μ H
M	Mutual inductance	300 μ H

In some references, a resistance has been chosen as a load for boost converters, but this is not correct for the boost converter used in the solar cell system [5,9,12,14,24,25]. In this system, the boost converter runs the MPPT algorithm, and its output voltage cannot be regulated. Therefore, the load should regulate the output voltage with the absorbing power from the DC link. In a real solar cell system, an inverter or battery bank, which are connected to the output of the solar converter, do this task properly. To simulate the behavior of the inverter or battery bank, a voltage-controlled current source was used as the load of the boost converter. Figure 9a shows the block diagram of the load, and the circuit of the voltage-controlled current source is shown in Figure 9b.

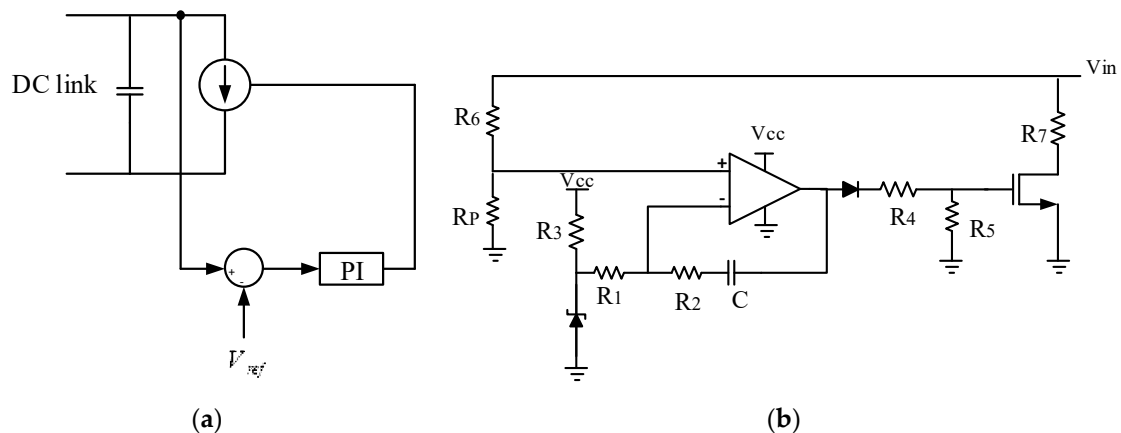


Figure 9. (a) Block diagram of the voltage-controlled current source, (b) circuit of the voltage-controlled current source.

The maximum power consumption of the load was 100 W and it adjusted the DC link voltage around 26 V.

Table 3 shows the MPPT algorithm parameters. To reduce the power oscillation to less than 0.1 W around the MPP, ΔV was calculated and resulted to be 4 mV according to Equation (14).

Table 3. Parameters of the maximum power point tracking (MPPT) algorithm.

Parameter	Value
ΔP_{max}	4 W
ΔP	0.1 W
ΔV	4 mV

4.1. Simulation Results and Analysis

The proposed MPPT algorithm was simulated in powersim (PSIM) for a 100 W solar cell. In the simulation, the performance of the system was studied at the sudden change of irradiation. It was assumed that the irradiation suddenly decreased from 1000 W/m² to 200 W/m² at 0.4 s and then increased to 1000 W/m² at 0.6 s. Figure 10 shows the simulation results. According to Figure 10b,c, the system tracked and found the MPP properly in and less than 2 ms. In addition, the MPPT efficiency was more than 99%.

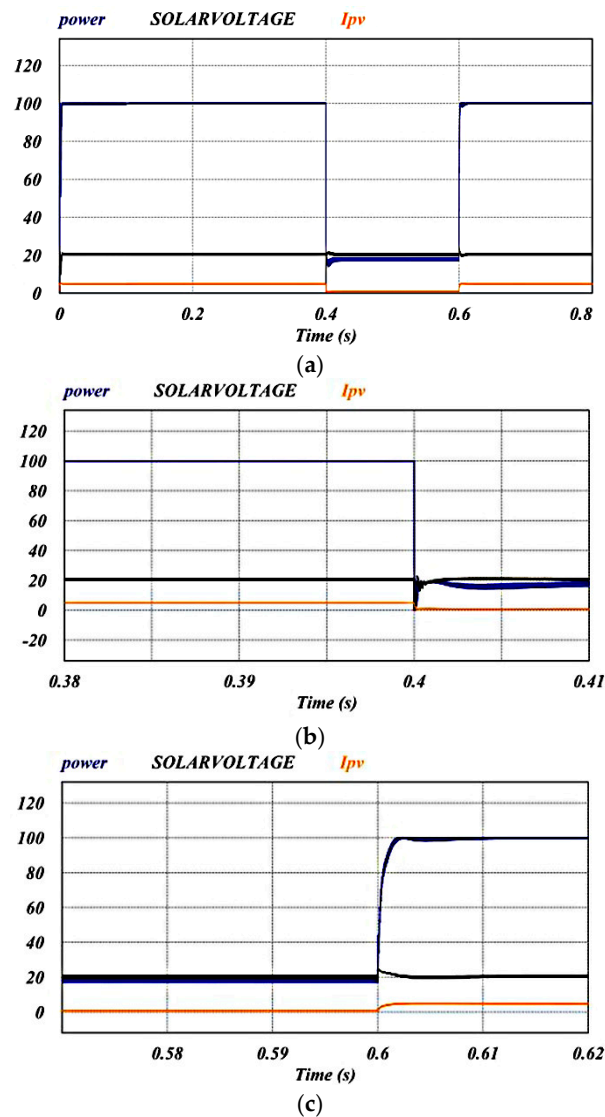


Figure 10. (a) Simulation results of power, voltage, and current with irradiation changes, (b) decreasing the irradiation, (c) increasing the irradiation.

4.2. Experimental Results and Analysis

To verify the performance of the new algorithm and the proposed converter, a 100 W prototype was implemented. The control unit of the system was implemented by a digital signal processor (DSP) TMS320F28335.

Because of the laboratory limitation, the solar irradiation was simulated by 12 incandescent lamps (220 V, 200 W). Figure 11 shows the solar cell prototype. The experimental results are shown in Figure 12, and the waveforms of power, voltage, and current are illustrated when the irradiation suddenly changed from the maximum to the minimum available irradiation and vice versa. The maximum and the minimum irradiation were 400 W/m^2 and 70 W/m^2 , respectively. According to Figure 12, the proposed algorithm tracking time was less than 4 ms and the system could find the MPP properly.

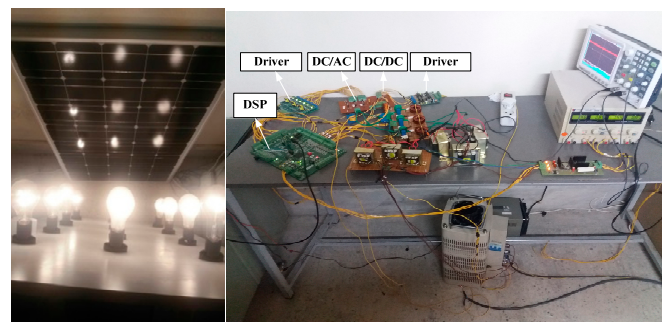


Figure 11. The implemented SC system in the laboratory.

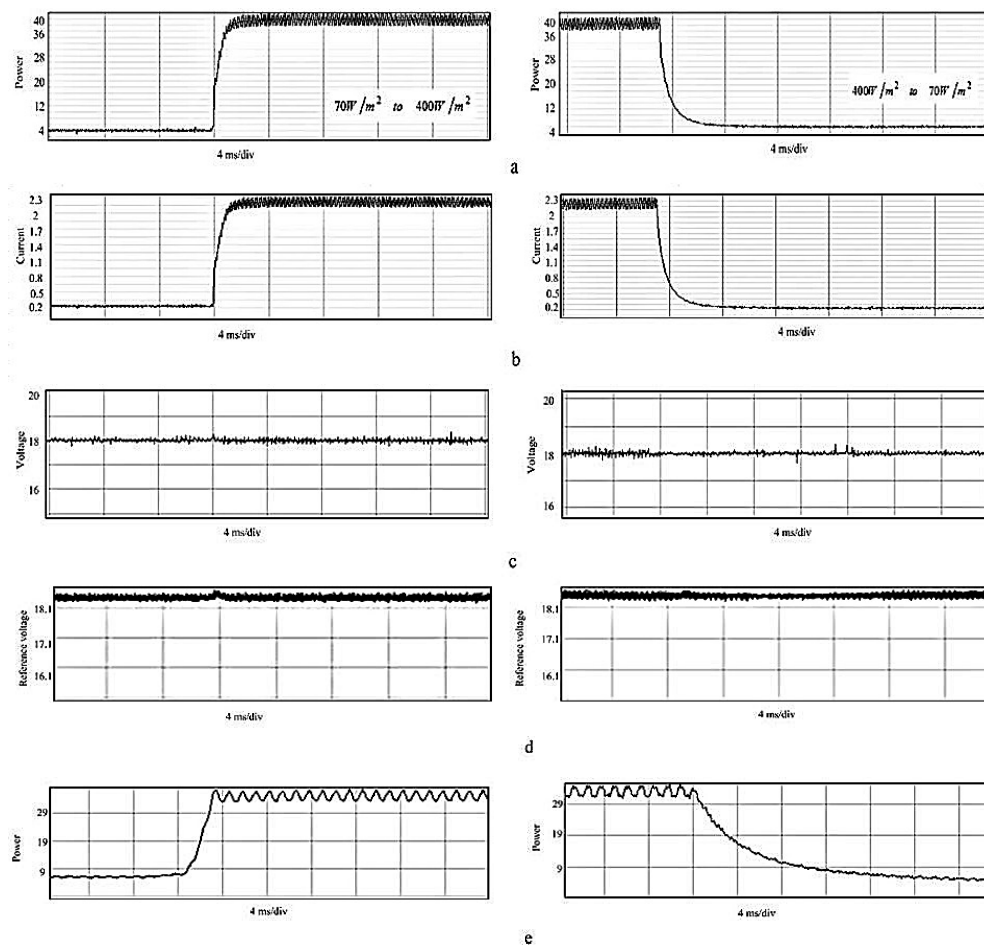


Figure 12. Experimental results with irradiation changes by the proposed algorithm (a) power, (b) current, (c) voltage, (d) reference voltage, (e) power by the P&O algorithm.

4.3. Comparative Study

To study the suitable performance of the proposed algorithm, the results were compared with those from the conventional algorithms. To compare in the same conditions, a cost function (CF) was defined for the converter. The cost function is the ratio of the energy stored in the converter to the maximum energy produced by the solar cell. The cost function is given as:

$$CF = \frac{C_{in} V^2 + LI^2}{P_{max}} \times f_{sw} \quad (16)$$

where P_{max} is the maximum power of the solar cell (W), C_{in} is the input capacitor (μF), V is the MPP voltage over the input capacitor (V), L is the inductor (mH), I is the current flows in the inductor at maximum power (A), and f_{sw} is the switching frequency (kHz).

The MPPT efficiency, tracking time, and cost function are presented in Table 4 for the proposed MPPT algorithm, conventional P&O and IC algorithms, and other references. It should be noted that, in this paper, the irradiation condition was worse than in other papers.

Table 4. The comparison between the proposed algorithm, conventional algorithms, and validated papers.

Algorithm	Time Tracking		MPPT Efficiency	Cost Function
	Decreasing Irradiation	Increasing Irradiation		
P&O	0.45 s	0.72 s	99%	29.87
IC	0.5 s	0.9 s	98%	164
[5]	0.36 s	0.82 s	99%	29.87
[9]	0.15 s	0.15 s	99%	164
[12]	0.25 s	0.25 s	99%	-
[24]	0.12 s	0.06 s	99%	29.87
[25]	0.05 s	0.05 s	99%	-
Proposed (CPV)	0.002 s	0.002 s	99%	2.17

According to Table 4, the time tracking of the proposed algorithm was at least 30 times less than in other papers, while the MPPT efficiency was 99%. According to the reform model, the cost function was at least 7 times less than in other papers. This shows that the volume of the passive elements of the proposed converter were 15 times smaller than in other studies.

Some simulation results with more details are presented below, based on architecture and on the proposed algorithm.

It was assumed that the irradiation decreased from 1000 W/m^2 to 200 W/m^2 at 0.4 s and then increased to 1000 W/m^2 at 0.6 s again. Figure 13 shows the simulation results under the proposed algorithm, combining the P&O and the CV algorithms, and the MPPT efficiency and tracking time are presented in Table 5.

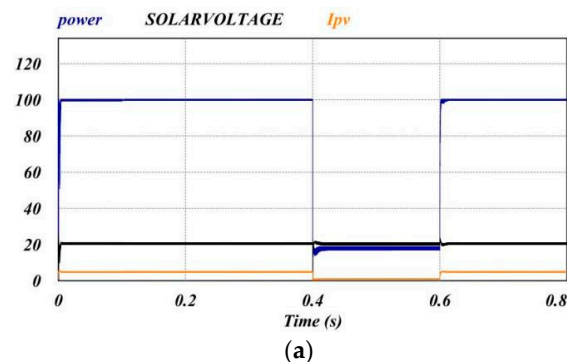


Figure 13. Cont.

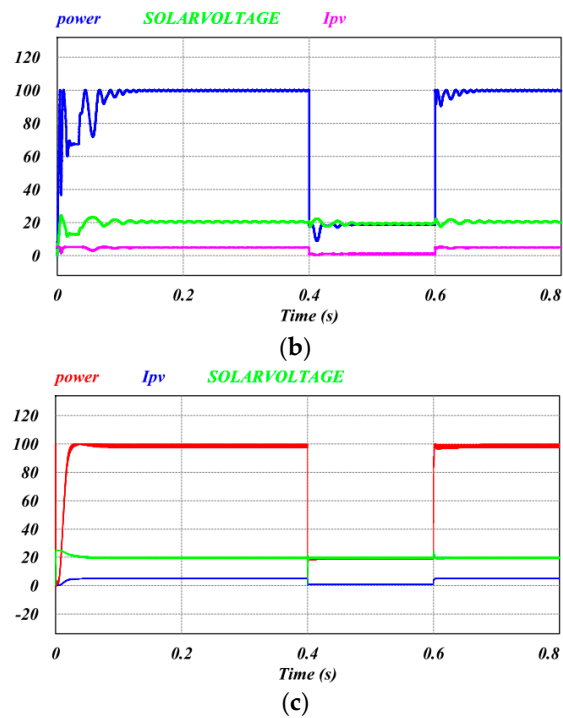


Figure 13. Simulation results of the power, voltage, and current under irradiation changes with (a) the proposed algorithm, (b) the P&O algorithm, and (c) the CV algorithm.

Table 5. The comparison between the proposed algorithm, the conventional algorithm, and the CV algorithm in terms of time tracking and efficiency.

Algorithm	Time Tracking		MPPT Efficiency
	Decreasing Irradiation	Increasing Irradiation	
P&O	0.02 s	0.032 s	98%
CV	0.002 s	0.002 s	95%
Proposed (CPV)	0.002 s	0.0024 s	99%

According to Table 1, time tracking and MPPT efficiency were improved with the proposed algorithm.

As shown in Figure 14, another irradiation condition was tested. It was assumed that the irradiation increased from 500 W/m² to 800 W/m² at 0.2 s and then increased to 1000 W/m² at 0.4 s. Afterwards, it decreased from 1000 W/m² to 800 W/m² at 0.6 s and from 800 W/m² to 600 W/m² at 0.8 s. As shown in Figure 14, the proposed algorithm was better than the conventional algorithm; therefore, the proposed algorithm has a fast speed and high efficiency under these conditions.

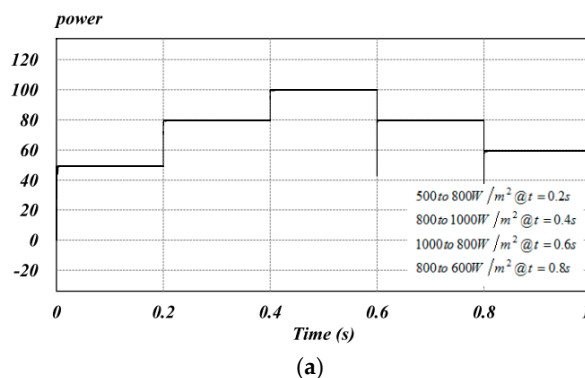


Figure 14. Cont.

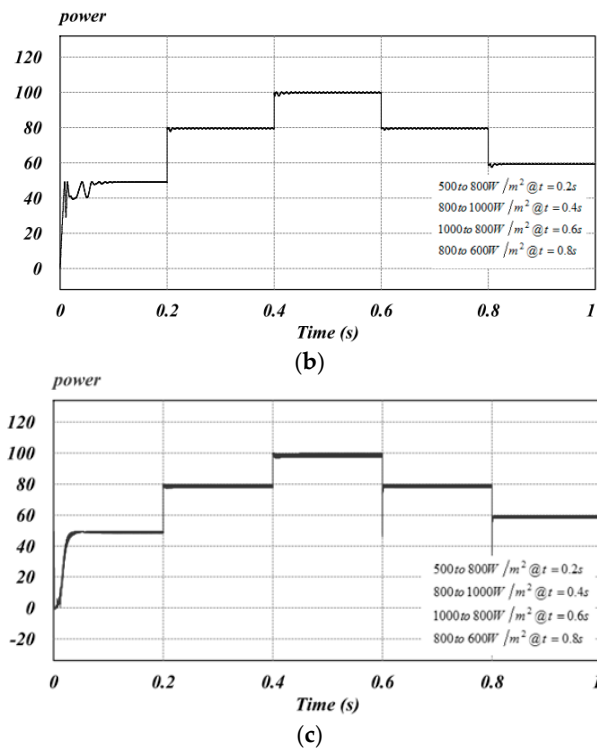


Figure 14. Simulation results of the power changes under irradiation changes with (a) the proposed algorithm (b), the P&O algorithm, (c) the CV algorithm.

More irradiation levels are considered in Figure 15, in which output power under the proposed method and the P&O and CV algorithms are reported:

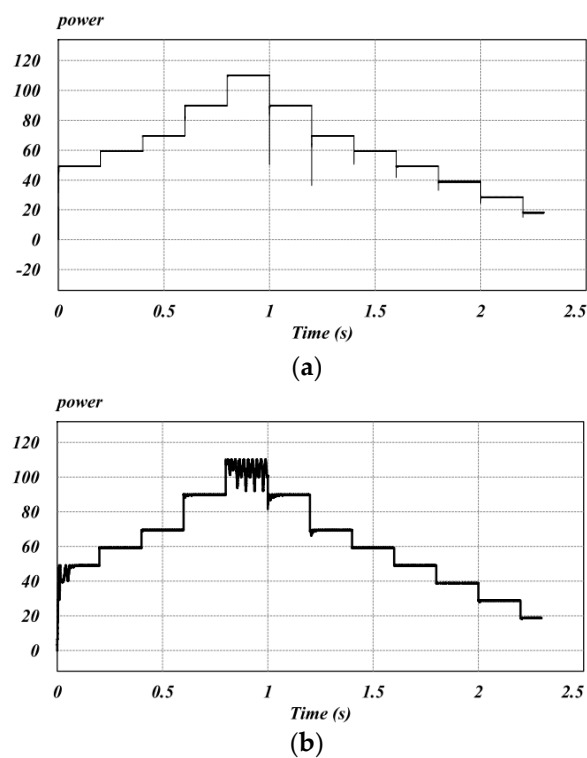


Figure 15. Cont.

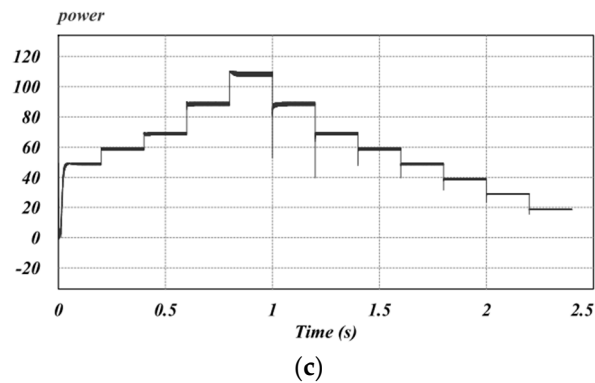


Figure 15. Simulation result of the power changes under irradiation changes with (a) the proposed algorithm, (b) the P&O algorithm, (c) the CV algorithm.

As shown in Figure 15, at the abrupt irradiation levels, the proposed algorithm tracked the MPP with high speed and high efficiency, but both the P&O and the CV algorithms did not have high performance.

As we discussed in the paper, choosing the appropriate structure leads to a lower cost function and does not require a bulk capacitor. However, high-speed tracking and high-MPPT efficiency are impossible by a conventional boost converter. In order to verify the performance of this type of converter, it was compared with a conventional converter with the same proposed algorithm.

It was assumed that the irradiation decreased from 1000 W/m^2 to 200 W/m^2 at 0.4 s and again increased to 1000 W/m^2 at 0.6 s. Figure 16a shows the simulation results with a selective converter, and Figure 16b shows the simulation results with a conventional boost converter. The MPPT efficiency and tracking time are presented in Table 2 for the proposed MPPT, the conventional P&O, and the CV. The comparative results are shown in Table 2.

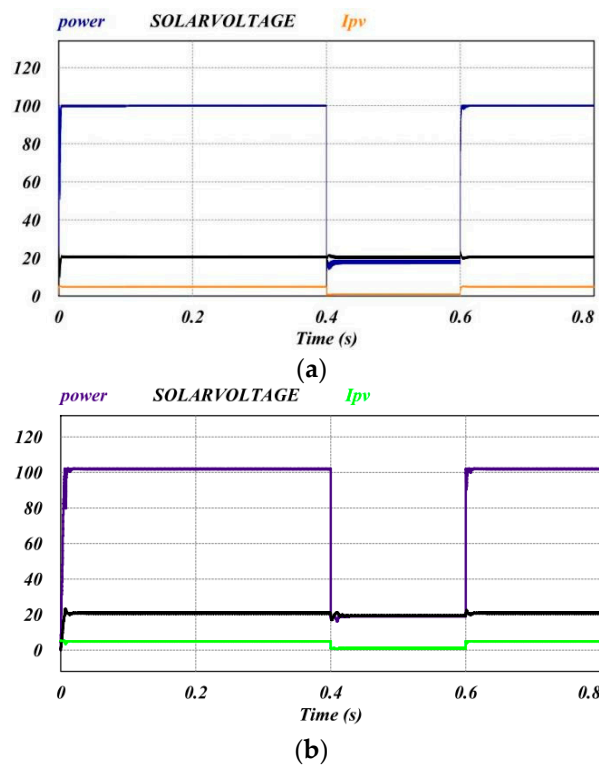


Figure 16. Simulation results of the power changes under irradiation changes with (a) the IBC converter, (b) a conventional converter.

According to Table 6, the results obtained by a conventional converter were the same with the selected structure if the input capacitor in the conventional boost converter was equal to 1000 μF , while the input capacitor in the selected converter was equal to 1 μF . Figure 17 was obtained by considering a conventional boost converter with a cost function equal to 2. As shown in this figure, it had a low performance (i.e., time tracking was 0.004 s, and efficiency was 91%).

Table 6. The comparison between a conventional and the interleaved boost converter (IBC) on the basis of the proposed algorithm.

Converter	Time Tracking		MPPT Efficiency
	Decreasing Irradiation	Increasing Irradiation	
Conventional	0.002 s	0.002 s	99%
IBC	0.002 s	0.002 s	99%

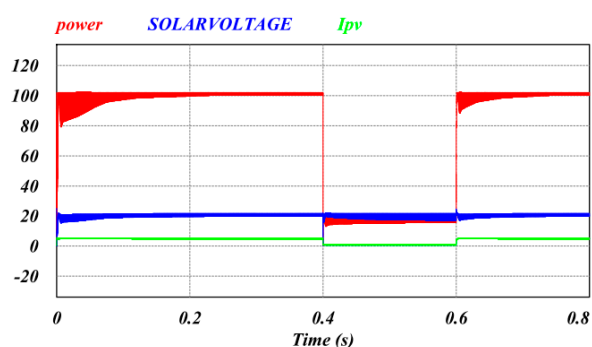


Figure 17. Simulation results of the power changes under irradiation changes with (a) the proposed algorithm, (b) the P&O algorithm.

Consequently, the proposed structure was effective for practical MPPT.

5. Conclusions

In this paper, the popular P&O and CV algorithms were used to obtain a fast response and a high MPPT efficiency. In the proposed algorithm, the CV algorithm regulates the operation point of the solar cell around the MPP when irradiation changes suddenly. Then, the P&O algorithm finds the exact MPP. Therefore, the new algorithm is an intelligent combination of the P&O and the CV algorithms. The simulation results of the 100 W prototype verified the performance of the proposed algorithm. The boost converter of the prototype was redesigned. It is a two-phase interleaved boost converter with a coupled inductor, which improved the conversion efficiency and minimized switching losses and the inherent switching ripple. To simulate the behavior of the inverter or battery bank, a voltage-controlled current source was used as the load of the boost converter. The experimental results showed that the tracking time was less than 2 ms, which is at least 30 times better than the time required by other conventional algorithms. In addition, a cost function (CF) was defined for the converter to compare the proposed method with other methods. The results showed that the cost function was about seven times lower than with other methods. Therefore, the volume of the passive elements was 15 times smaller than in other studies.

Author Contributions: All authors contributed equally to this work and all authors have read and approved the final manuscript.

Funding: This research received no external funding.

Conflicts of Interest: The authors declare no conflicts of interest.

References

1. Rahmanian, E.; Akbari, H.; Sheisi, G.H. Maximum power point tracking in grid connected wind plant by using intelligent controller and switched reluctance generator. *IEEE Trans. Sustain. Energy* **2017**, *8*, 1313–1320. [[CrossRef](#)]
2. De Brito, M.A.G.; Galotto, L.; Sampaio, L.P.; e Melo, G.D.A.; Canesin, C.A. Evaluation of the main mppt techniques for photovoltaic applications. *IEEE Trans. Ind. Electron.* **2013**, *60*, 1156–1167. [[CrossRef](#)]
3. Femia, N.; Petrone, G.; Spagnuolo, G.; Vitelli, M. Optimization of perturb and observe maximum power point tracking method. *IEEE Trans. Power Electron.* **2005**, *20*, 963–973. [[CrossRef](#)]
4. Sera, D.; Mathe, L.; Kerekes, T.; Spataru, S.V.; Teodorescu, R. On the perturb-and-observe and incremental conductance mppt methods for pv systems. *IEEE J. Photovolt.* **2013**, *3*, 1070–1078. [[CrossRef](#)]
5. Kollimalla, S.K.; Mishra, M.K. A Novel Adaptive P&O MPPT Algorithm Considering Sudden Changes in the Irradiance. *IEEE Trans. Energy Convers.* **2014**, *29*, 602–610. [[CrossRef](#)]
6. Ahmed, J.; Salam, Z. A modified p&o maximum power point tracking method with reduced steady-state oscillation and improved tracking efficiency. *IEEE Trans. Sustain. Energy* **2016**, *7*, 1506–1515. [[CrossRef](#)]
7. Macaulay, J.; Zhou, Z. A Fuzzy Logical-Based Variable Step Size P&O MPPT Algorithm for Photovoltaic System. *Energies* **2018**, *11*, 1340. [[CrossRef](#)]
8. ESRAM, T.; Chapman, P.L. Comparison of photovoltaic array maximum power point tracking techniques. *IEEE Trans. Energy Convers.* **2007**, *22*, 439–449. [[CrossRef](#)]
9. Mei, Q.; Shan, M.; Liu, L.; Guerrero, J.M. A novel improved variable step-size incremental-resistance mppt method for pv systems. *IEEE Trans. Ind. Electron.* **2011**, *58*, 2427–2434. [[CrossRef](#)]
10. Faranda, R.; Leva, S. Energy comparison of mppt techniques for pv systems. *WSEAS Trans. Power Syst.* **2008**, *3*, 446–455.
11. Dallago, E.; Liberale, A.; Miotti, D.; Venchi, G. Direct mppt algorithm for pv sources with only voltage measurements. *IEEE Trans. Power Electron.* **2015**, *30*, 6742–6750. [[CrossRef](#)]
12. Killi, M.; Samanta, S. An adaptive voltage-sensor-based mppt for photovoltaic systems with sepic converter including steady-state and drift analysis. *IEEE Trans. Ind. Electron.* **2015**, *62*, 7609–7619. [[CrossRef](#)]
13. Adly, M.; El-Sherif, H.; Ibrahim, M. Maximum power point tracker for a pv cell using a fuzzy agent adapted by the fractional open circuit voltage technique. In Proceedings of the IEEE International Conference in Fuzzy Systems (FUZZ), Taipei, Taiwan, 27–30 June 2011; pp. 1918–1922.
14. Tousi, S.R.; Moradi, M.H.; Basir, N.S.; Nemati, M. A function-based maximum power point tracking method for photovoltaic systems. *IEEE Trans. Power Electron.* **2016**, *31*, 2120–2128. [[CrossRef](#)]
15. Teng, J.H.; Huang, W.H.; Hsu, T.A.; Wang, C.Y. Novel and fast maximum power point tracking for photovoltaic generation. *IEEE Trans. Ind. Electron.* **2016**, *63*, 4955–4966. [[CrossRef](#)]
16. Manuel Godinho Rodrigues, E.; Godina, R.; Marzband, M.; Pouresmaeil, E. Simulation and Comparison of Mathematical Models of PV Cells with Growing Levels of Complexity. *Energies* **2018**, *11*, 2902. [[CrossRef](#)]
17. Kumar, K.K.; Bhaskar, R.; Koti, H. Implementation of mppt algorithm for solar photovoltaic cell by comparing short-circuit method and incremental conductance method. *Procedia Technol.* **2014**, *12*, 705–715. [[CrossRef](#)]
18. Al Nabulsi, A.; Dhaouadi, R. Efficiency optimization of a dsp-based standalone pv system using fuzzy logic and dual-mppt control. *IEEE Trans. Ind. Inform.* **2012**, *8*, 573–584. [[CrossRef](#)]
19. Kim, H.; Kim, S.; Kwon, C.K.; Min, Y.J.; Kim, C.; Kim, S.W. An energy-efficient fast maximum power point tracking circuit in an 800- μ w photovoltaic energy harvester. *IEEE Trans. Power Electron.* **2013**, *28*, 2927–2935. [[CrossRef](#)]
20. Raj, J.C.M.; Jeyakumar, A.E. A novel maximum power point tracking technique for photovoltaic module based on power plane analysis of I–V characteristics. *IEEE Trans. Ind. Electron.* **2014**, *61*, 4734–4745. [[CrossRef](#)]
21. Espinoza-Trejo, D.R.; Bárcenas-Bárcenas, E.; Campos-Delgado, D.U.; De Angelo, C.H. Voltage-oriented input–output linearization controller as maximum power point tracking technique for photovoltaic systems. *IEEE Trans. Ind. Electron.* **2015**, *62*, 3499–3507. [[CrossRef](#)]
22. Hong, Y.; Pham, S.N.; Yoo, T.; Chae, K.; Baek, K.H.; Kim, Y.S. Efficient maximum power point tracking for a distributed pv system under rapidly changing environmental conditions. *IEEE Trans. Power Electron.* **2015**, *30*, 4209–4218. [[CrossRef](#)]
23. Streetman, B.G. *Solid State Electronic Devices*; Prentice Hall: Upper Saddle River, NJ, USA, 2005.

24. Kollimalla, S.K.; Mishra, M.K. Variable perturbation size adaptive p&o mppt algorithm for sudden changes in irradiance. *IEEE Trans. Sustain. Energy* **2014**, *5*, 718–728. [[CrossRef](#)]
25. Moo, C.S.; Wu, G.B. Maximum power point tracking with ripple current orientation for photovoltaic applications. *IEEE J. Emerg. Sel. Top. Power Electron.* **2014**, *2*, 842–848. [[CrossRef](#)]



© 2019 by the authors. Licensee MDPI, Basel, Switzerland. This article is an open access article distributed under the terms and conditions of the Creative Commons Attribution (CC BY) license (<http://creativecommons.org/licenses/by/4.0/>).